Possible experiments to distinguish between different methods of treating the Pauli principle in nuclear potential models

D. Krolle, H. J. Assenbaum, C. Funck, and K. Langanke

Institut für Theoretische Physik I, Universität Münster, Münster, Federal Republic of Germany

The finite Pauli repulsion model of Walliser and Nakaichi-Maeda and the orthogonality condition model are two microscopically motivated potential models for the description of nuclear collisions which, however, differ from each other in the way they incorporate antisymmetrization effects into the nucleus-nucleus interaction. We have used $\alpha + \alpha$ scattering at low energies as a tool to distinguish between the two different treatments of the Pauli principle. Both models are consistent with the presently available on-shell (elastic) and off-shell (bremsstrahlung) data. We suggest further measurements of $\alpha + \alpha$ bremsstrahlung including the coplanar laboratory differential cross section in Harvard geometry at α-particle angles of around 27° and the γ-decay width of the 4^+ resonance at $E_{c.m.} = 11.4$ MeV, because in both cases the two models make significantly different predictions.

I. INTRODUCTION

The $\alpha + \alpha$ system has served for a long time as a well-studied tool to understand the nuclear interaction between composite particles and to learn about the effects of the Pauli principle on the relative motion of the fragment nuclei. Buck et al.[1] constructed an l-independent $\alpha + \alpha$ potential of Gaussian form factor with which they were able to describe the elastic $\alpha + \alpha$ data at energies $E \leq 15$ MeV. Based on the idea of the orthogonal condition model (OCM)[2] they incorporated the repulsive effect of the Pauli principle into their model via the picture of the Pauli forbidden states,[3] which they simulated by unphysical bound states in the potential. The treatment of the Pauli principle by Pauli forbidden states originates from microscopic many-body theories of nuclear collisions describing the fragment nuclei by their respective harmonic oscillator ground state wave functions (with equal width parameters) in which case it is possible that the relative wave function of the fragments has to be orthogonal to certain states (the Pauli forbidden states), or otherwise, these components will lead to vanishing many-body wave functions caused by antisymmetrization. For the $\alpha + \alpha$ system these microscopic theories result in two (one) Pauli forbidden states for the $l = 0$ ($l = 2$) relative wave function, while there is no Pauli forbidden state in the higher partial waves.

Although the potential of Ref. 1 reproduces the on-shell properties of the 2α system very well, it gives rise, on the other hand, to the 3α overbinding problem. This means the ground state energy of the 3α system calculated using the potential[1] of Buck et al. as an effective $\alpha + \alpha$ interaction is lower by roughly 7 MeV compared to the experimental binding energy of the ^{12}C nucleus and should become even lower if the model space for the ^{12}C nucleus is not restricted only to that of a configuration of three α particles. Although the 3α overbinding problem throws some shadow onto the justification of the $\alpha + \alpha$ potential of Ref. 1, it in itself, however, does not bare enough evidence to rule out this particular $\alpha + \alpha$ potential as the

overbinding can also be explained by the existence of a repulsive 3α interaction.

Recently, Walliser and Nakaichi-Maeda[4] showed that the 3α overbinding problem can also be solved if in the $\alpha + \alpha$ interaction the Pauli repulsion is not described by the orthogonality to strictly Pauli forbidden states—or in other words, by the truncation of that part of relative motion space which is spanned by the Pauli forbidden states—but rather by a nonlocal repulsion term of finite strength allowing also those states which are forbidden in the OCM description to play a role in the dynamics of the system. Combining this description of the Pauli repulsion with an attractive local $\alpha + \alpha$ potential of Gaussian form, Walliser and Nakaichi-Maeda were able to determine the on-shell properties of the 2α system (which they did by comparing their results with those of the Buck et al. potential rather than with experimental data as they did not include the Coulomb interaction within their study) and simultaneously to approximate the energies of the two lowest 0^+ levels in ^{12}C very well.

Based on this remarkable success, the treatment of the Pauli principle in the finite Pauli repulsion model (FPRM), as the authors called their model, might be viewed superior to the one of the OCM. However, because of the imponderability introduced by the third α particle, the ^{12}C system does not allow one rigorously to distinguish between the two different ways of describing the Pauli repulsion. Since we believe that this question is of vivid interest to the entire field of nuclear collisions between composite fragments, it should be settled experimentally using a test case which allows for stricter conclusions. We will argue in this paper that studying nuclear bremsstrahlung in the $\alpha + \alpha$ system at energies $E \leq 15$ MeV provides such a suited test case, whereby our argumentation runs as follows: It is well known that α particles are relatively compact and that the γ channel is the only open channel in the $\alpha + \alpha$ system at $E \leq 15$ MeV. These facts leads us to the conclusion that for studying low-energy $\alpha + \alpha$ bremsstrahlung, other fragmentations of the eight-nucleon system can be safely neglected. The

same is true for internal contributions of the α particles considering the various quantum numbers of their ground state. One therefore expects that in this energy regime nuclear bremsstrahlung in the $\alpha+\alpha$ system arises from transitions between $\alpha+\alpha$ relative wave functions and might give unambiguous information about the effects of the Pauli principle. On the other hand, the above given considerations allow us to study $\alpha+\alpha$ bremsstrahlung at $E \leq 15$ MeV in the framework of a nuclear potential by employing the effective interactions of the OCM and of the FPRM and by looking for different predictions of the two models. We have performed such potential model calculations and, in fact, found that the bremsstrahlung cross sections calculated on the basis of the OCM and FPRM deviate from each other up to a magnitude which is detectable by present day experimental techniques.

We would like to mention that Ref. 5 reports a similar study to the present one discussing the different treatments of the Pauli principle in the OCM and in phenomenological models which simulate the Pauli principle by a repulsive core.

Our paper is organized as follows. In Sec. II we will give a brief description of the potential model for nuclear bremsstrahlung, while the results of our calculation as well as our conclusions are presented in Sec. III.

II. THEORETICAL BACKGROUND

The following presentation of the theoretical background of our study follows closely the outline given by Refs. 5—7. In Ref. 7 Baye and Descouvemont have developed a microscopic model to study nuclear bremsstrahlung, while subsequently in Ref. 5, a potential model of structureless particles has been presented on the basis of their theory. Both models have been applied to the $\alpha+\alpha$ system; the deviations between their results could be explained in terms of differences in the nuclear phase shifts, therefore demonstrating that a reproduction of the (experimental) phase shifts is an important ingredient in any meaningful study of nucleus-nucleus bremsstrahlung and that an explicit consideration of internal degrees of freedom is not necessary for the $\alpha+\alpha$ system.[5] We will study in the following, the low-energy $\alpha+\alpha$ bremsstrahlung in the nuclear potential model of Ref. 5 employing the $\alpha+\alpha$ interaction of Buck et al. and of Walliser and Nakaichi-Maeda (including a Coulomb part) which both reproduce the experimental $\alpha+\alpha$ phase shifts for $E \leq 15$ MeV. Note that the nuclear potential model has also been successfully used in the study of nuclear bremsstrahlung for other nuclear systems.[8,9]

The γ transition under consideration is of $E2$ type. Hence the differential bremsstrahlung cross section $d\sigma/dE$ from an $\alpha+\alpha$ scattering state at energy E_i in the partial wave l_i into a final state at energy E_f with angular momentum l_f emitting a photon of energy $E_\gamma = E_f - E_i$ is given by[5,7]

$$\frac{d\sigma}{dE_\gamma} = \frac{80e^2(2l_f+1)}{3(\hbar c)^2 k_i^3 k_f k_\gamma}(l_f 200 \,|\, l_i 0)^2 \,|\, I(\tfrac{1}{2}k_\gamma)\,|^2 \,, \quad (1)$$

where k_i, k_f are the wave numbers in the initial and final scattering states, respectively, and k_γ is the wave number

of the photon $(E_\gamma = \hbar c k_\gamma)$. The radial matrix element is defined as[5]

$$I(k) = 6 \int_0^\infty dx\, g_{l_f}(x) j_2(kx) \frac{d}{dx} \left[\frac{1}{x} g_{l_i}(x) \right]$$

$$- \tfrac{1}{2}[l_f(l_f+1) - l_i(l_i+1) - 6]$$

$$\times \int_0^\infty dx \frac{1}{x^2} g_{l_f}(x) g_{l_i}(x) \frac{d}{dx}[x j_2(kx)] \,, \quad (2)$$

where j_2 is the spherical Bessel function of order 2. The relative wave functions g_l are determined by solving the Schrödinger equation of relative motion

$$\left\{ -\frac{\hbar^2}{2\mu}\left[\frac{d^2}{dx^2} - \frac{l(l+1)}{x^2} \right] + V_C(x) - E \right\} g_l(x)$$

$$= - \int dx' V(x,x') g_l(x') \quad (3)$$

using either the $\alpha+\alpha$ potential of Buck et al.,[1]

$$V(x,x') = V_0 \exp\left[-\frac{x^2}{a^2} \right] \delta(x-x') \,,$$

$$(V_0 = -122.6225 \text{ MeV}, \ a = 2.132 \text{ fm}) \,, \quad (4)$$

or a potential based on the FPRM,[4]

$$V(x,x') = V_0 \exp\left[-\frac{x^2}{a^2} \right] \delta(x-x') + \sum_\nu a_\nu \phi_\nu^*(x) \phi_\nu(x') \,,$$

$$(a = 2.132 \text{ fm}) \,, \quad (5)$$

and adopting the Coulomb potential $V_C(x)$ from Ref. 1. The strength parameter V_0 in Eq. (5) is determined below. The second part describes the Pauli repulsion of finite strength. It is a sum over those oscillator states forbidden in the conventional OCM picture [these are the $(0s)$ and $(1s)$ states in the partial wave $l=0$ and the $(0d)$ state in partial wave $l=2$]; however, differing from the latter as the strength parameters a_ν are finite $(a_{0s}=8\hbar\omega,$ $a_{0d}=a_{1s}=4\hbar\omega,$ $\hbar\omega=12.3$ MeV, Ref. 4) rather than infinity as the OCM. For the width of the oscillator wave functions Walliser and Nakaichi-Maeda adopt $b=1.4$ fm. Note that the potential of Ref. 1 can also be written in form of Eq. (5), adopting the wave functions ϕ_ν as the bound states of the potential (4) and letting the parameters a_ν approach infinity $(a_\nu \to \infty)$.

The scattering states in Eq. (3) are normalized asymptotically to

$$g_l(x) \to I_l(kx) - \exp[2i(\delta_l + \sigma_l)]O_l(kx) \quad (6)$$

with $I_l = (O_l)^* = \exp(i\sigma_l)(G_l - iF_l)$, where F_l and G_l are the regular and irregular Coulomb functions, respectively; δ_l, σ_l are the nuclear and Coulomb phase shifts. Note that the integrals in (3) have been evaluated numerically, improving their convergence by employing the contour integration method of Ref. 10.

Finally we are interested in the coplanar laboratory differential cross section in Harvard geometry where the latter imposes the following conditions on the angles of the α particles in the laboratory frame $[\Omega_i = (\theta_i, \phi_i),$

$i = 1,2$] and on the angle of the photon [$(\Omega_\gamma = (\theta_\gamma, \phi_\gamma)$], for which we assume that it is identical in the laboratory system and in the c.m. system: $\theta_1 = \theta_2$, $\phi_1 = \phi_2 = \phi_\gamma = 0, \pi$. The photon angle θ_γ is not observed in these experiments.

The desired cross section in Harvard geometry can be most easily calculated starting from the coplanar laboratory cross section which is given by[5,7]

$$\frac{d^3\sigma}{d\Omega_1 d\Omega_2 d\theta_\gamma} = -8\pi \frac{p_1^4 v_f \sin^2\theta_1 \sin^2\theta_2}{(2\pi\hbar)^4 \hbar \sin^5(\theta_1 + \theta_2)} \sum_{\substack{l_i l_i' \\ l_f l_f'}} X_{l_i l_f} X_{l_i' l_f'}^* \sum_{jj'J} (2 2\, 1\, -1 \mid j\, 0)(l_f l_f' 00 \mid j'\, 0)(l_i l_i' 00 \mid J\, 0)$$

$$\times \begin{Bmatrix} l_f & 2 & l_i \\ l_f' & 2 & l_i' \\ j' & j & J \end{Bmatrix} [Y_j(\Omega_\gamma) \otimes Y_{j'}(\Omega_f)]_0^J . \tag{7}$$

The momentum of the incident particle is p_1; v_f is the relative velocity in the exit channel. The various c.m. variables appearing in (7) have to be calculated as functions of the laboratory angles, which in Harvard geometry is rather straightforward, yielding[7]

$$E_\gamma = E_i(1 - \tan^2\theta_1) ,$$
$$\Omega_f = 0 . \tag{8}$$

Finally, the quantities $X_{l_i l_f}$ are defined in the present case as

$$X_{l_i l_f} = i^{l_i - l_f + 2} \frac{40\pi}{\sqrt{12}} (2l_f + 1)(2l_i + 1)$$

$$\times \exp[2i(\delta_{l_f} + \sigma_{l_f})] \frac{e}{ck_\gamma} \begin{pmatrix} l_f & 2 & l_i \\ 0 & 0 & 0 \end{pmatrix}$$

$$\times \left[\frac{1}{k_i k_f}\right]^{3/2} I(\tfrac{1}{2} k_\gamma) . \tag{9}$$

The coplanar laboratory differential cross section is then obtained from Eq. (7) by integration over the photon angle θ_γ and by multiplication with a factor 2 to account for the case of identical nuclei.

III. RESULTS

The first step we have to take in evaluating the bremsstrahlung cross sections is to calculate the $\alpha + \alpha$ relative wave functions in the initial and final states. However, in doing so we face the problem that the $\alpha + \alpha$ potential has been determined in Ref. 4 without considering the Coulomb interaction and has consequently been compared previously only to other theoretical results rather than to experimental data. Although the Coulomb interaction is known to be rather small in the $\alpha + \alpha$ system we found that by simply adding the Coulomb potential, which has been used in Ref. 1, to the FPRM interaction does not reproduce the experimental $\alpha + \alpha$ phase shifts well enough to allow for a meaningful study of nuclear bremsstrahlung. We have therefore refitted the local part of the FPRM potential by adjusting its strength parameter to the

experimental $\alpha + \alpha$ phase shifts and by adopting the Coulomb part of the $\alpha + \alpha$ potential from Ref. 1. We find that by slightly lowering the depth of the local Gaussian potential to $V_0 = -118.065$ MeV (in Ref. 4 the parameter $V_0 = -117.427$ MeV has been used) the experimental phase shifts in the partial waves $l = 0$ and $l = 2$ are well reproduced at energies $E \leq 15$ MeV including the broad 2^+ resonance at $E = 2.9$ MeV. Furthermore, we can state that the potential exhibits a narrow resonance in the partial wave $l = 0$ corresponding to the experimental ^{8}Be ground state at $E = 92.1$ keV with an experimental width of $\Gamma = 6.8 \pm 1.7$ eV.[11] However, due to numerical inaccuracies, we are not able to determine the exact energy position of this resonance in the FPRM. Note that this is at variance with the potential of Buck et al., which is known to reproduce the properties of the ^{8}Be ground state resonance. The numerical inaccuracies are caused by the fact that the FPRM potential is nonlocal, while the potential of Ref. 1 is a local one [see Eqs. (4) and (5)].

The FPRM potential as determined for the partial waves $l = 0,2$ does not reproduce the experimental phase shifts in the partial waves $l \geq 4$. Since it is the goal of the present paper to derive some experimentally detectable differences in the $\alpha + \alpha$ bremsstrahlung cross sections caused by the different treatments of the Pauli principle in the conventional OCM picture and the FPRM and since there are no effects of the Pauli principle in partial waves $l \geq 4$ in both models, we simply adopt the potential of Ref. 1 for determining the relative wave functions in the partial waves $l \geq 4$. In Fig. 1 we compare the $\alpha + \alpha$ phase shifts calculated with the potential of Buck et al. and within the FPRM using the presently adjusted potential with the experimental phase shifts. Based on the experiences given in Ref. 5, the reproduction of the experimental data is good enough in both cases to be confident that possible differences showing up in the bremsstrahlung cross sections calculated on the basis of the two models are not caused by trivial differences in the nuclear phase shifts.

Having determined the initial and final nuclear wave functions, we are able to calculate the bremsstrahlung cross sections. Considering that the only experimental in-
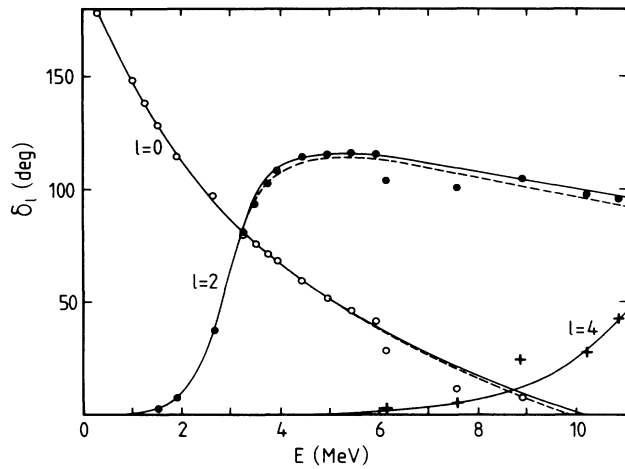
FIG. 1. Comparison of the $\alpha+\alpha$ phase shifts calculated from the potential of Buck *et al.* (Ref. 1, solid line) and from the present FPRM potential (dashed line) with the experimental phase shifts (Ref. 14) in the partial waves $l=0$ (open circles) and $l=2$ (solid circles). In the partial wave $l=4$ (squares) the two potentials have been assumed to be identical.

vestigations of $\alpha+\alpha$ bremsstrahlung at low energies have been performed in Harvard geometry choosing the laboratory angles to be $\theta_1=35°$ and $\theta_1=37°$ (Refs. 12 and 13), we have calculated the corresponding coplanar laboratory differential cross sections at these angles to check at first whether the two different $\alpha+\alpha$ interactions of Refs. 1 and 4 are consistent with the existing experimental data. The calculated cross sections are displayed in Fig. 2. Several observations are important for the present study as we will discuss in the following:

(1) For both $\alpha+\alpha$ potentials the overall agreement with the data at $\theta_1=35°$ (Ref. 12) is good; they also produce the data at $\theta_1=37°$ (Ref. 13) for $E_i<6.5$ MeV. As has been pointed out similarly in Refs. 5 and 9, the calculations do not show the structure seen in the experimental cross sections at $E_i\approx6.5$ MeV. In Refs. 5 and 7 it was doubted
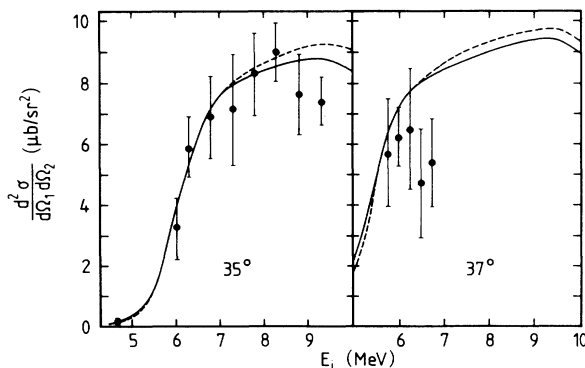
that this structure has a physical reality.

(2) The two potentials result in nearly identical cross sections at energies $E_i\leq7.5$ MeV for $\theta_1=35°$ and at $E\leq7$ MeV for $\theta_1=37°$; at higher energies the cross sections calculated withing the FPRM are always slightly larger than calculated for the $\alpha+\alpha$ potential of Ref. 1.

Combining the observations (1) and (2), we like to conclude that both potentials are consistent with the presently available data and more experimental information is needed to distinguish between the two different treatments of the Pauli principle. In the following we want to discuss where to look for in future experiments.

To understand what kind of experiments we are looking for, one has to recognize that it is the effect of the Pauli principle on the relative wave functions we are after. It is well known that the effects of the Pauli principle are short ranged and therefore one can only expect to find clues about how the Pauli principle influences the relative wave functions, if the experiment is set up also to probe the nuclear interior region. To get an impression about the deviations caused by the different treatment of the Pauli principle in the OCM and in the FPRM, we have displayed the $l=0$ and $l=2$ scattering states at $E=3$ MeV as calculated in the two models in Fig. 3. Note that the $l=2$ state is at resonance at this energy. One clearly observes from Fig. 3 that the range of the Pauli principle is roughly 3.5 fm; for separations larger than that, the two respective wave functions are identical as they are calculated from phase-equivalent potentials. For distances $x\leq3.5$

FIG. 2. Laboratory differential cross sections in the Harvard geometry at $\theta_1=\theta_2=35°$ and 37° calculated from the potential of Buck *et al.* (Ref. 1, solid line) and in the FPRM (dashed line). The experimental data are from Refs. 12 and 13.
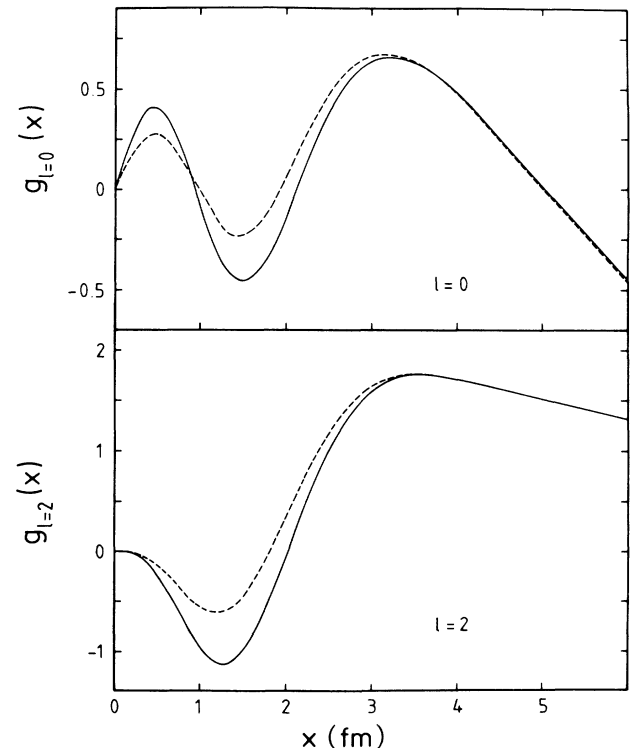
FIG. 3. Comparison of scattering wave functions at $E=3$ MeV in the partial waves $l=0$ and 2 calculated from the potential of Buck *et al.* (Ref. 1, solid line) and in the FPRM (dashed line). The vertical scale is in arbitrary units.

fm the Pauli repulsion is active in both models leading to the typical nodal structure in the wave functions associated with the Pauli forbidden states. However, one also observes that the different treatment of the Pauli principle in the two models results in slightly different positions of the nodes and in different amplitudes of the oscillations in the wave functions at short distances. One can therefore expect that experiments which involve transitions from or into $l=0$ or $l=2$ nuclear states (remember that there are no effects of the Pauli principle in the partial waves $l \geq 4$) and which are sensitive to the nuclear interior region $x \leq 3.5$ fm might allow one to distinguish between the two suggested treatments of the Pauli repulsion. We will discuss in the following that this is indeed the case, but first we like to mention that for the desired experimental distinction it is not sufficient that only one of the nuclear states involved is at resonance, while the other is nonresonant.

This supposition is confirmed by the results shown in Fig. 2. The strong increase of the cross sections in the energy range $E_i \approx 5-7$ MeV is caused by the fact that the capture transitions in this energy regime lead partially to the broad 2^+ resonance in the final channel. However, we do not find differences in the predicted cross sections calculated from the potential of Buck *et al.* and in the FPRM caused by the fact that the initial states in this energy regime are all nonresonant.[5]

To look for suited inter-resonant transitions in the $\alpha+\alpha$ system, one has to consider that in the OCM as well as in the FPRM a Pauli repulsion is only active in the partial waves $l=0$ and $l=2$. This suggests that one should look for the present purposes for experiments which are sensitive to the electromagnetic transitions between the lowest 2^+ and 0^+ states and lowest 4^+ and 2^+ states in ^{8}Be.

Ideally one likes to measure the γ width of the 2^+ resonance in ^{8}Be at $E=2.94$ MeV, as in this case the nuclear interior region of both the initial and final states are affected by the Pauli principle. Unfortunately we were not able to calculate within the FPRM the $E2$ transition from the 2^+ resonance into the ^{8}Be ground state due to the above mentioned numerical problems we had with the final narrow resonant state.

However, we are able to make some quantitative predictions about the expected outcome of future experiments involving the resonant transition from the broad 4^+ resonance in ^{8}Be at $E \approx 11$ MeV into the 2^+ state at $E=2.94$ MeV. One possible kind of experiment is to measure the laboratory differential cross sections in Harvard geometry choosing the angle θ_1 appropriately. Note that in the previous experiments the angles correspond to ratios $E_\gamma/E_i=0.43$ ($\theta_1=37°$) and 0.51 ($\theta_1=35°$) and hence the discussed resonant transitions have not been observed in full strength. It should, however, be emphasized that the difference between the laboratory cross sections calculated from the potential of Ref. 1 and in the FPRM for angles $\theta_1=35°,37°$ and at energies $E_i \geq 8$ MeV (see Fig. 2) are caused by the onset of the resonant transition as the corresponding energies correspond to transitions from the low energy wing of the 4^+ resonance into the high energy wing of the 2^+ state.
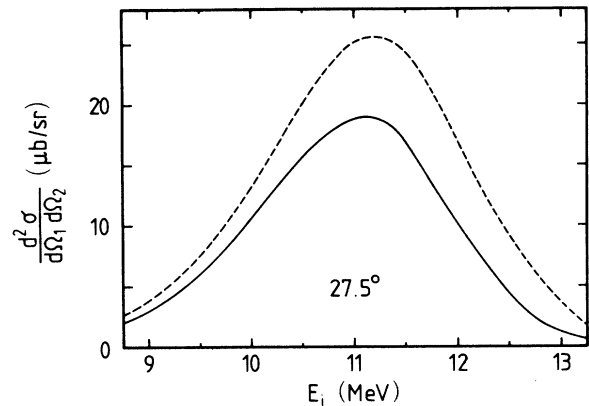
FIG. 4. Laboratory differential cross sections in the Harvard geometry at $\theta_1=\theta_2=27.5°$ calculated from the potential of Buck *et al.* (Ref. 1, solid line) and in the FPRM (dashed line).

To match the two resonances optimally the angle θ_1 should be chosen as $\theta_1 \approx 27.5°$ ($E_\gamma/E_i \approx 0.73$). In Fig. 4 we have displayed the laboratory differential cross sections in Harvard geometry for this angle calculated for the potential of Ref. 1 and in the FPRM. The cross sections for both potential sets clearly exhibit a resonant structure reflecting the dominance of the 4^+ to 2^+ transition. More interesting for the present discussion is the finding that the FPRM predicts over the entire energy range larger cross sections than the potential of Buck *et al.* On top of the 4^+ resonance, the FPRM estimates a
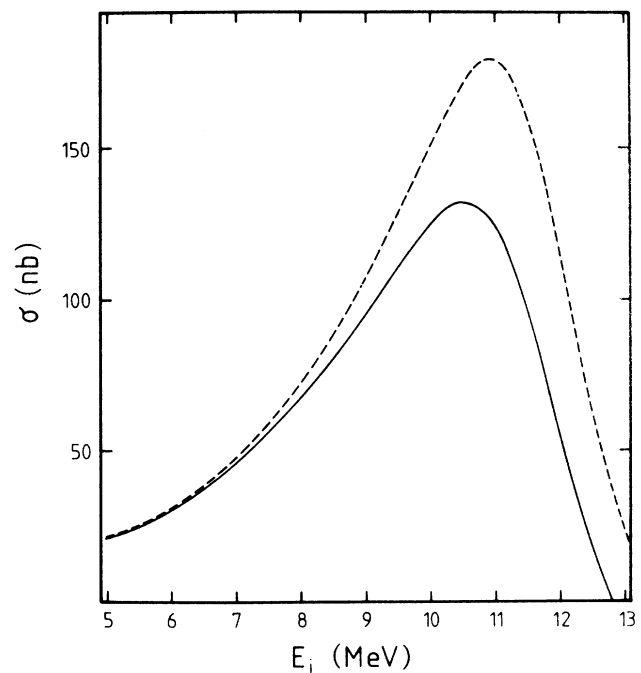
FIG. 5. Bremsstrahlung cross sections for the transition from the 4^+ resonance in the entrance channel into the 2^+ resonance in ^{8}Be, integrated over the energies of the final resonance, as calculated from the potential of Ref. 1 (solid line) and in the FPRM (dashed line).

cross section of roughly 26 μb/sr^2 which is some 35% larger than the predictions of the potential of Buck *et al.* (19 μb/sr^2). Based on experimental accuracy achieved in the measurements of the cross sections at $\theta_1 = 35°$ and $\theta_1 = 37°$, we are quite convinced that the differences in the cross sections predicted by the two models are large enough to be resolved by a measurement of the laboratory cross sections in Harvard geometry at $\theta_1 = 27.5°$.

Another experiment which allows us to distinguish between the two different treatments of the Pauli principle is the determination of the γ width of the 4^+ resonance at $E \approx 11$ MeV due to $E2$ decay. We have calculated the γ width of the 4^+ resonance from Eq. (1) by integrating over the energies of the final 2^+ resonance covering the range $E_f = 2-4$ MeV. Our results are shown in Fig. 5. We find a maximum cross section on top of the resonance

of ≈ 130 nb for the potential of Ref. 1 and of ≈ 180 nb within the FPRM. Approximating the $\sigma(E)$ cross sections near the resonance energy by a Breit-Wigner parametrization, we find the quotient $\Gamma_\gamma/\Gamma_{tot} \approx 1.2 \times 10^{-7}$ for the potential of Buck *et al.* and $\approx 1.7 \times 10^{-7}$ in the FPRM. Adopting the calculated α width of the 4^+ resonance as its total width ($\Gamma_\alpha \approx 3.85$ MeV), these ratios correspond to γ widths of $\Gamma_\gamma \approx 0.45$ eV (19 W.u.) and of ≈ 0.64 eV (26 W.u.), respectively. Again, we are convinced that the differences in the predictions of the two models are large enough to be resolvable by experiment. Such experiments might be either direct measurements of the capture cross sections or indirect measurements in which reactions like ^{11}B(p,α)^{8}Be are used to populate the 4^+ resonance, and then the $\Gamma_\gamma/\Gamma_{tot}$ ratio is determined from α-γ-coincidence measurements.

[1]B. Buck, H. Friedrich, and C. Wheatley, Nucl. Phys. A275, 246 (1977).

[2]S. Saito, Prog. Theor. Phys. Suppl. 62, 11 (1978).

[3]S. Saito, Prog. Theor. Phys. 41, 705 (1969).

[4]H. Walliser and S. Nakaichi-Maeda, Nucl. Phys. A464, 366 (1987).

[5]K. Langanke, Phys. Lett. 174B, 27 (1986).

[6]R. J. Philpott and D. Halderson, Nucl. Phys. A375, 169 (1982).

[7]D. Baye and P. Descouvement, Nucl. Phys. A443, 302 (1985).

[8]D. Krolle and K. Langanke, Z. Phys. A (to be published).

[9]D. Krolle, K. Langanke, and M. Stingl (unpublished).

[10]C. M. Vincent and H. T. Fortune, Phys. Rev. C 2, 782 (1970).

[11]F. Ajzenberg-Selove, Nucl. Phys. A320, 1 (1979).

[12]U. Peyer, J. Hall, R. Müller, M. Suter, and W. Wölfli, Phys. Lett. 41B, 151 (1972).

[13]B. Frois, J. Birchall, C. R. Lamontagne, U. v. Möllendorf, R. Roy, and R. J. Slobodrian, Phys. Rev. C 8, 2132 (1973).

[14]S. A. Afzel, A. A. Z. Ahmed, and S. Ali, Rev. Mod. Phys. 41, 247 (1969).